Mechanical Behaviour of Thermoplastic Composites Spot-Welded and Mechanically Fastened Joints: A Preliminary Comparison

Tian Zhao[1*], Genevieve Palardy[1*], Irene Fernandez Villegas[1*], Calvin Rans[1*], Marcias Martinez[2*], Rinze Benedictus[1*]

1) Structural Integrity Group, Faculty of Aerospace Engineering, Delft University of Technology, Netherlands

2) Department of Mechanical & Aeronautical Engineering, Clarkson University, Potsdam, New York, USA

Corresponding author: T.Zhao@tudelft.nl

Abstract

The in-plane and out-of-plane mechanical behaviour of both ultrasonically spot-welded and mechanically fastened joints was investigated by double-lap shear and pull-through tests, respectively. Spot-welded specimens showed comparable onset failure load and significantly higher joint stiffness compared to mechanical fasteners when carrying shear load. The failure modes and the damage within specimens were analysed after mechanical tests. Intralaminar failure and very limited damage on the out-most ply were found for welded specimens, whereas catastrophic through-the-thickness failure was observed for mechanically fastened joints. Based on the experimental outcomes, the mechanical performance and failure mechanisms of spot-welded joints were critically assessed in comparison to the mechanical fasteners .

Keywords: A. Thermoplastic resin, B. Mechanical properties, D. Fractography, E. Joints/joining

1. Introduction

In the latest decades, thermoplastic composites (TPCs) have become increasingly interesting for their use on aircraft structures owing to the superior strength- and stiffness-to-weight ratios in comparison to metals and cost-effective manufacturing process in comparison to thermoset composites

(TSCs) [1-3]. Apart from these benefits, TPCs can be welded. This is due to the intrinsic property of thermoplastic resins that they can be melted when being heated and retain their original mechanical properties after cooling down [3-5]. On one hand, welding techniques can be classified based on the heating mechanisms [3], namely friction welding, thermal welding and electromagnetic welding. On the other hand, based on the welded area, welding techniques can be generally divided into two groups, i.e. continuous welding and spot welding. The well-known induction and resistance welding are typically continuous welding techniques. They are currently applied in the aerospace industry for the joining of thermoplastic composite parts [6, 7] as a composite-friendly alternative to mechanically fastened joints [3-6, 8]. Similarly to adhesively bonded joints, continuously welded seams in thermoplastic composite structures do not require drilling of holes in the adherends and avoid stress concentrations resulting from point load introduction. Contrarily to adhesive bonding, welding relies on polymer autohesion at the welding interface and hence it does not depend on adhesion mechanisms of difficult inspectability. Ultrasonic welding is also known as a very interesting technique for joining thermoplastic composites with a number of advantages over resistance and induction welding, such as very short welding times, very low energy consumption, highly concentrated heat generation and potential for in-situ process monitoring [6, 9, 10]. One of its main limitations is that it is traditionally a spot welding technique and, hence, as opposed to continuous welding techniques it does not avoid point load introduction in the welded joint. On the positive side, spot welding could be expected to decrease assembly times as well as to provide joints with a crack arresting nature.

Spot welded joints are current practice in metallic constructions/structures such as automotive industries. The main metal spot welding techniques are resistance spot welding (RSW) , friction stir spot welding (FSSW) and ultrasonic spot welding (USW). Both RSW and FSSW have been extensively used and studied by many researchers for decades [11, 12]. RSW was attractive because of its ease of operation and low costs and was regarded as the predominant process for joining conventional pressed steel [11, 13, 14]. FSSW was developed in 1991 and was first used for the joining of aluminium and its alloys. It is energy efficient and is capable of joining components of any shapes and dissimilar materials [12, 13]. Compared to FSSW and RSW, USW was shown to have even shorter welding cycles (typically < 0.4 s), less energy consumption and higher efficiency. Therefore, USW has been of increased interest for many

researchers and numerous research has been carried out on its application on the assembly of steels and alloys [13-17]. Apart from that, a couple of investigations were carried out on applying spot welding on joining metal and thermoplastic composites. An experimental research was performed by P. Mistschang [18] on metal (Steel DC01 and Aluminium Al/Mg3) and carbon fibre reinforced polymer composites (CFRPC). Induction spot welding was used to bond the metal/CFRPC and the mechanical performance of welded joints was characterized by single-lap tests. The experimental outcomes showed that the lap-shear strength (LSS) of welded joints created by induction spot welding reached around 85% of the adhesive bonded joints in the same condition and highlighted the short welding process (< 2 min). However, the results also indicated that the weld strength of induction spot welding was greatly influenced by the pre-treatments on the metal substrates. Besides, the welding time of ultrasonic welding, normally less than 10 s, is significantly shorter than induction welding. More recently, F. Balle [19] investigated the lap-shear mechanical properties and failure modes of hybrid joints consisting of different aluminium alloy (AA1050, AA5754 and AA2024) and thermoplastic composites (CF/PA66 and CF/PEEK) created by ultrasonic spot welding. The test results showed high quality welded joints between metal and CFRPC. There is however very little knowledge on spot welding of thermoplastic composite structures, both in terms of manufacturing process and mechanical performance. This knowledge gap needs to be overcome to facilitate the future industrial application of TPC spot welding.

As the basis for further research and development on the topic, this paper focuses on the static in-plane and out-of-plane behaviour of single-spot welded joints as compared to joints with a single mechanical fastener. Following usual procedures in composite mechanically fastened joints [20-23], the in-plane behaviour is characterised through double lap shear tests and the out-of-plane behaviour through pull-through tests. The damage affected zones (DAZ) are assessed using cross-section microscopy [22] and ultrasonic inspection [23]. Cross-section microscopy and fractography are used to analyse the failure mechanisms.

2. Experimental

2.1. Mechanical testing and evaluation

Double-lap shear (DLS) tests were performed to evaluate the in-plane failure and mechanical performance of both spot-welded and mechanically fastened joints since the effect of out-of-plane bending can be effectively diminished in this configuration [20, 21]. Specimens were comprised of four composite plates (114.4 × 25.4 mm^2) with a square overlap area of 25.4× 25.4 mm^2, as shown in Fig. 1. Therefore, both a spot-welded and a mechanically fastened joint could be created in the central point of the overlap. The tests were carried out on a Zwick/Roell 250kN universal testing machine. Specimens were clamped with hydraulic grips and loaded until failure with a crosshead speed of 1.3 mm/min in accordance with ASTM D3528-96 [24]. To guarantee a safe failure mode and avoid an over distortion of the specimens, tests were stopped when a 30% load drop from the maximum attained value was found [25]. Five specimens were tested for both types of joints.

The out-of-plane performance of both welded and mechanically fastened joints was evaluated with pull-through (PT) tests following ASTM D7332-09 [26]. Specimens consisting of two square composite plates assembled with either a spot weld or a mechanical fastener were placed in between a pair of loading fixtures (see Fig. 2). The size of the composite plates is shown in Fig. 2. To accommodate the test fixture, four holes were drilled on each plate prior to the assembly and the top plate was joined at a 45° angle with respect to the bottom one. A compressive load was applied on the fixture with a Zwick/Roell 250kN universal testing machine, which resulted in a tensile force on the joints. Specimens were loaded with a crosshead displacement rate of 0.5 mm/min and the tests were stopped following the 30% load drop principle as well. Five specimens were tested for both types of joints.

Load-displacement (L-D) curves recorded during the tests were utilized to characterize the mechanical behaviour of both types of joints. As illustrated in [20, 23, 27], the loading process of the mechanically fastened specimens normally shows two failure points, namely onset failure and ultimate failure. In this study, both of the load values on these two points were noted, hereafter mentioned as onset failure load (OFL) and ultimate failure load (UFL), to evaluate the load-carrying capability of the joints. The OFL was calculated by the bilinear approximation method, which is commonly used in

numerical modelling to characterize the structural failure and proved to provide good fits to the experimental L-D curves [28, 29]. An example is shown on representative DLS (a) and PT (b) L-D curves for mechanically fastened joints in Fig. 3. Linear fitting was performed on the stages before and after the stiffness reduction and the OFL was located at the intersection of two fitting lines. According to the statement in ASTM D7332 [26], OFL of specimens in PT tests is regarded as the first peak load during the loading process in correspondence with a significant load drop (more than 10%). However, the first obvious load drop for all mechanically fastened specimens was found to be lower than 10%, which will be mentioned in Section 3.2. Therefore, to keep consistent with the results in DLS tests, the OFL of the mechanically fastened joint is also calculated by using the bilinear approximation method. The UFL is recorded by the maximum load point on the L-D curves. Additionally, the linear fitting of the initially elastic stage of L-D curves corresponds to the joint stiffness (JS), which is another interesting mechanical property for the comparison between the welded and the mechanically fastened joints in this study.

Fracture surfaces were inspected using a Zeiss Stereo Microscope. Further fracture analysis was carried out on welded specimens with a JSM-7500F Scanning Electron Microscope (SEM). Finally, the Damage Affected Zone (DAZ) as well as the through-the-thickness failure within specimens were evaluated via a C-scan and also cross-sectional optical microscopy.

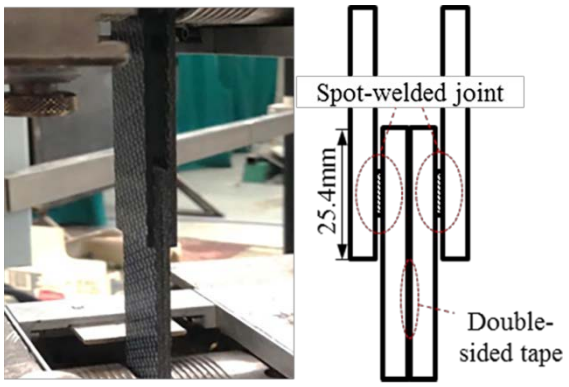

(a)

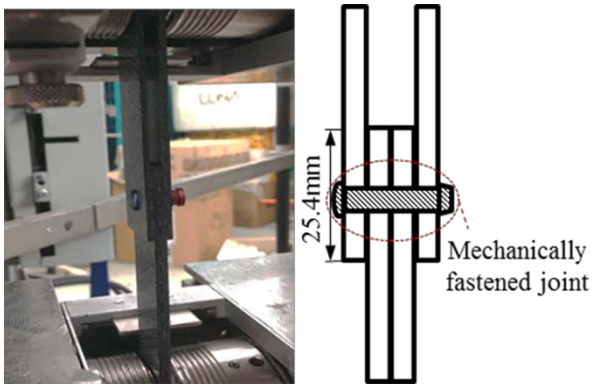

(b)

Fig. 1. Loading fixture and specimen configurations for DLS tests: (a) spot-welded specimen; (b) mechanically fastened specimen.

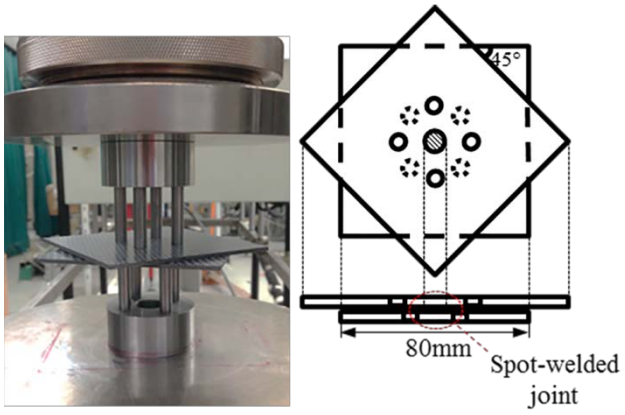

(a)

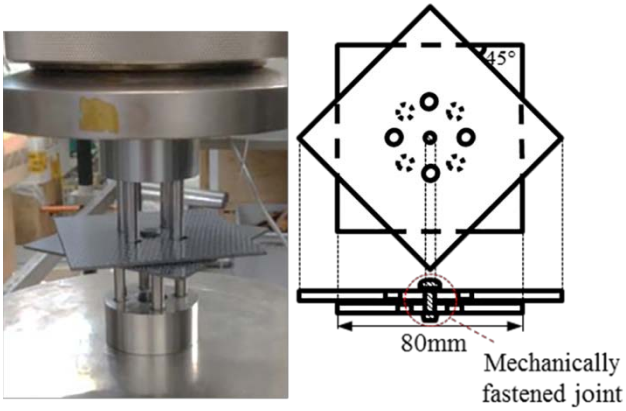

(b)

Fig. 2. Loading fixture and specimen configurations for PT tests: (a) spot-welded specimen; (b) mechanically fastened specimen.

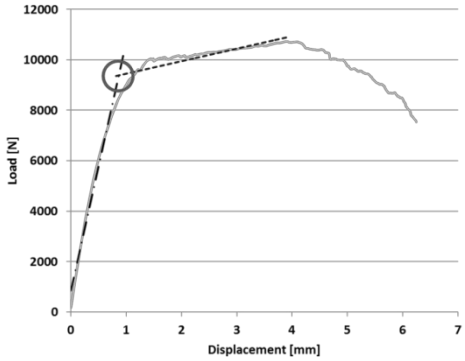

(a)

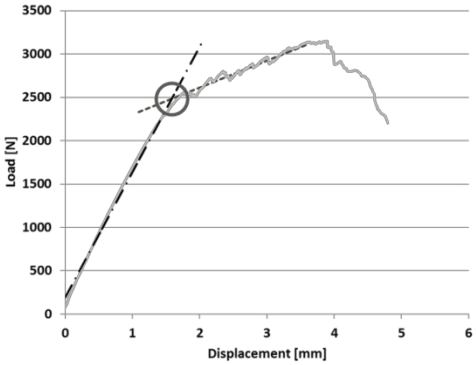

(b)

Fig. 3. Bilnear approximation (dashed lines) for the OFL of mechanically fastened joints in DLS (a) and PT (b) tests. OFL is indicated by the circles on the intersection of two fitting lines.

2.2. Laminates

The material used in this study was 5 harness satin fabric CF/PEEK (carbon fibre-reinforced poly-ether-ether ketone), which was supplied by TenCate Advanced Composites, The Netherlands. Six-ply laminates with dimensions of 580 mm × 580 mm and with a $[0/90]_{3s}$ stacking sequence, were consolidated in a hot-platen press. The preimpregnated stacks were sandwiched between two aluminium plates and were compression moulded at 385°C and 1 MPa for 20 min. The final thickness of the laminates was approximately 1.90 mm. Afterwards, specimens were cut into the required dimensions according to the test procedures, i.e. DLS and PT tests, with a water cooled diamond saw.

2.3. Assembly techniques

2.3.1. Ultrasonic Welding

A 20 kHz Rinco Dynamic micro-processor controlled ultrasonic welder was employed in this study to weld individual specimens. Fig. 4 shows the welding set-up equipped with a 10 mm-diameter cylindrical sonotrode. This titanium sonotrode was shown to be appropriate for spot welding as any secondary welding outside of the intended welding area was effectively prevented. Two different custom-made welding jigs were utilized to accommodate the specimen configurations for either the DLS or the PT tests, as shown in Fig. 4(a) and (b), respectively. Specifically in this study, adherends were first single-lap welded on the welding jig in Fig. 4(a). Then, the DLS specimens were created with a pair of single-lap specimens by using double-sided tape, as shown in Fig. 1(a). An energy-controlled mode was adopted in this research for the spot welding. Based on knowledge gathered from preliminary experimental results, 600J input energy with 1500N welding force and 60.8 µm peak-to-peak amplitude were used as the welding parameters during the vibration period in this study. Afterwards, the joints were allowed to consolidate at 1500 N for 4.0 s.

Spot flat energy directors, made of a neat resin film, were used to create the spot-welded joints in this study, as shown in Fig. 5. To keep consistent with the pin diameter of the mechanical fasteners, 4 mm-diameter-circular energy directors (EDs) were used, as cut from the PEEK film with a nominal thickness of 0.25 mm. Prior to the welding process, the spot EDs were manually fixed on the bottom adherend with a Rinco handheld ultrasonic welder. The ED melted, flowed and created a bigger spot-welded joint (approximately 10mm in diameter) during the welding process, which will be illustrated in detail in Section 3.1.

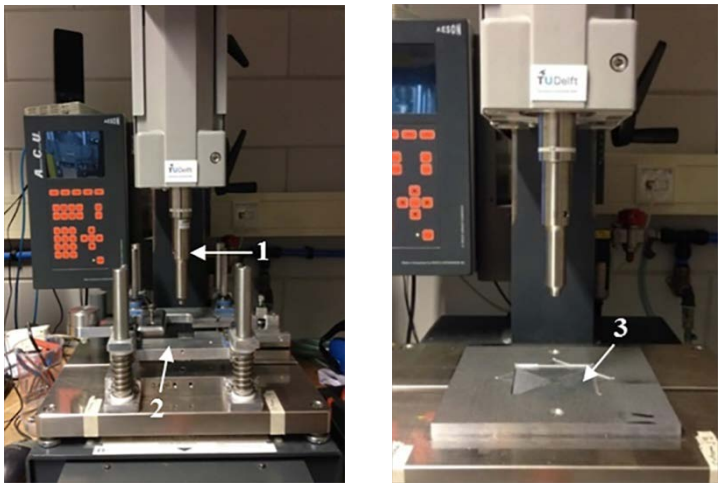

(a) (b)

Fig. 4. Ultrasonic welder and welding jigs used in this study. 1: circular sonotrode with a diameter of 10 mm, 2: welding jig for DLS specimens, 3: welding jig for PT specimens.

Fig. 5. Spot energy director fixed on composite adherend prior to welding process.

(a) (b)

Fig. 6. Schematic of the Hi-Lok® fasteners utilized in the mechanical tests: (a) HL10V6; (b) HL12V6.

2.3.2. Mechanical fastening

Titanium Hi-Lok® fasteners HL10V6 and HL12V6 (protruding head for both) were used to join the composite adherends for the DLS and PT tests, respectively. As indicated in Fig. 6, both of these two

models of fasteners have a 4.8 mm-diameter-pin, which is close to the diameter of the spot energy director (4 mm). In addition, the 7 mm length pin of the HL10V6 fastener is well-suited for the installation of four composite adherends, which has an overall thickness of around 7.6 mm. The HL12V6 fatener has a 9.3 mm-diameter-head, which is designed for carrying peel load and approximately equal to the diameter of the spot welds (approximately 10 mm). Hi-Lok® fasteners were manually installed with a ratchet wrench, following [30]. The installation of Hi-Lok® fasteners was completed by the failure of the collar's wrenching device [30], providing a consistent clamping force for all of the mechanically fastened joints.

3. Results and discussion

3.1. Mechanical behaviour of both types of joints in DLS tests

A comparison of representative DLS L-D curves between the spot-welded and mechanically fastened joints is summarized in Fig. 7. The black solid line corresponding to the spot-welded specimen exhibits a linear behaviour with a continuous load increase and no obvious reduction of the joint stiffness observed until ultimate failure. On the contrary, the loading history of mechanically fastened specimen with a HL10V6 fastener (the grey dashed line) shows different stages, which is in good agreement with the study in [20]. Basically, four different stages can be observed from the L-D curve: (1) the load linearly increases in the initial period until the obvious slope/stiffness alternation. Although the load transfer mechanisms are different in this stage, due to the very small change of the stiffness, the first two stages illustrated in [20] are regarded as one stage; (2) the joint stiffness keeps on decreasing while the load continues to increase due to the presence of bearing damage; (3) the load almost keeps constant until the maximum point (UFL), illustrating the joint slowly losing load-carrying capability with the evolution of bearing damage; (4) the load has a continuous drop which indicates the ultimate failure of the joint.

Table 1 lists the average OFL, UFL and JS of both types of joints, accompanied by the corresponding coefficient of variation (COV) in the parentheses. Since the welded specimens failed immediately after the maximum load was reached, only UFL was represented. As mentioned in Section

2.1, the OFL of mechanically fastened joints, which is more important in the structural design rather than the UFL [23], was calculated by using bilinear approximation. It is notable that the OFL of both types of joints in DLS tests are within the same range, which is also indicated by the bar graph in Fig. 8. The variation of the load-carrying capability of both types of joints are within standard deviation, which is displayed by the error bars. In contrast, the averaged stiffness of spot-welded joints is reported to be substantially higher, by 88%, than the mechanically fastened specimens. In addition, the COV is lower for the spot-welded joints.

To figure out the main cause for the stiffness reduction in the mechanically fastened joints, tensile tests were carried out on CF/PEEK composites coupons with and without the central hole. Fig. 9 shows the experimental results. It can be noted that, compared to intact composite coupons, the stiffness reduction of central-cut coupon (approximately 12%) is not as significant as the stiffness difference observed in DLS tests. Therefore, the stiffness degradation observed in the mechanically fastened joints is likely induced by the concentrated pin-load applied on the interior of the circumference of the bolted hole during the DLS tests.

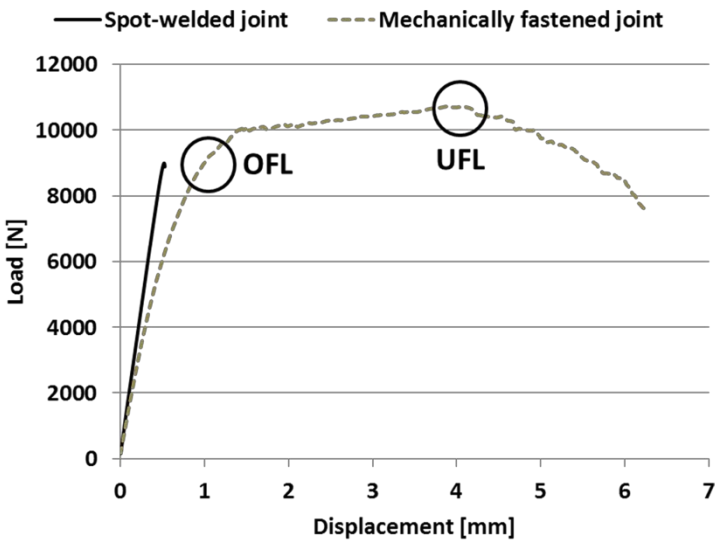

Fig. 7. Comparison of representative Load-displacement curves between spot-welded (solid line) and mechanically fastened (dashed line) joints in DLS tests. The left and right circles indicate the onset and ultimate failure, respectively. The data are adopted from [31].

Table 1
Experimental results on both types of joints for DLS tests.

Joint type	Average OFL (N) (COV %)	Average UFL (N) (COV %)	Average JS (N/mm) (COV %)
Spot-welded joints	-	9645.9 (10.6)	17954.4 (3.0)
Mechanically fastened joints (HL10V6)	9190.7 (9.2)	10403.6 (7.5)	9542.5 (7.3)

(OFL: onset failure load, UFL: ultimate failure load, JS: joint stiffness, COV: coefficient of variation)

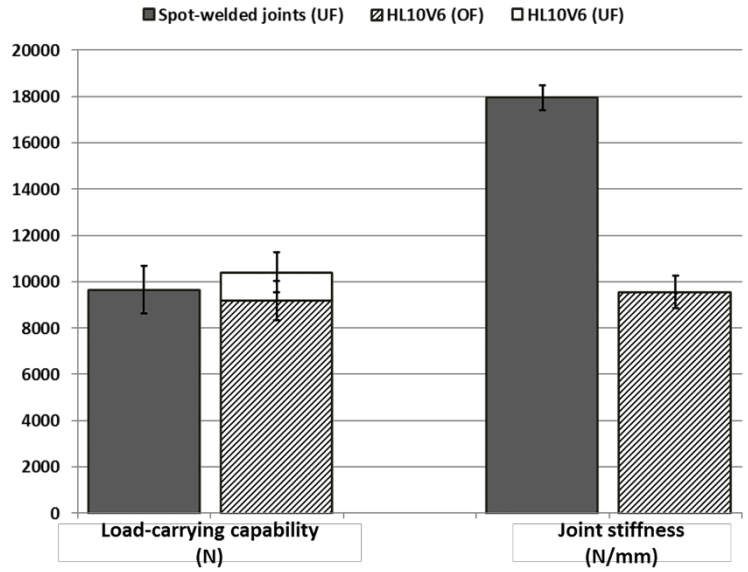

Fig. 8. Comparison of in-plane mechanical (shear) performance for both types of joints in DLS tests. (OF: onset failure, UF: ultimate failure) The error bars indicate the standard deviation.

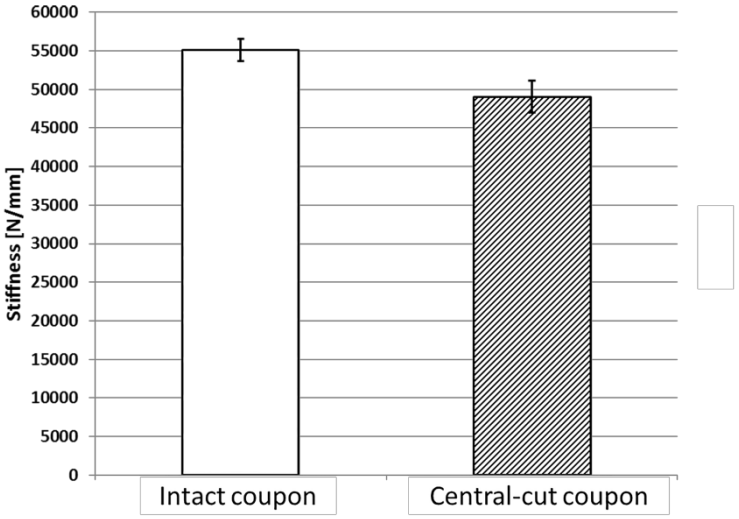

Fig. 9. Comparison of stiffness between intact and central-cut coupon in tensile test.

Regarding the fracture surfaces, a post-mortem visual inspection of the welded specimens indicated the presence of a circular welded joint on the overlap, as shown in Fig. 10(a). The diameter of the spot-welded joints was found to be approximately 10 mm on average, which is about 150% and 108% in excess of the original ED (4 mm) and the pin of the Hi-Lok® fastener (4.8 mm), respectively. The rest of the overlap remains intact and no further damage is observed. Intralaminar failure was confirmed by the SEM analysis, following the high quality of the bond created during the welding process [32]. This failure mode is represented by tearing of fibre bundles of the out-most laminate ply (Fig. 10(b)) and fibre-matrix debonding (Fig. 10(c)). A further magnification of Fig. 10(c) is shown in Fig. 10(d), providing a better observation on the separation between fibres and thermoplastic resin, indicating the fibre-matrix debonding.

Mechanically fastened specimens after DLS tests are illustrated in Fig. 11. Due to the penetration of the fastener during the loading process, a catastrophic bearing failure is found on the composite adherends. Fig. 11(a) and (b) show the top and bottom sides of the mechanically fastened specimen, respectively. Two cracks are observed on the outer plates, propagating towards the edges of the overlap, indicating that shear-tear out failure will eventually take place in the composite plates. Fig. 11(c) and (d) provide a clear view of bearing failure on the adherends after removing the mechanical fastener, which is similar to the observation in [20]. However, both outer and inner plates show obvious

bearing damage together with elongated bolted holes. The possible explanation could be that the total thickness of the four composite adherends is slightly larger than the pin length of the Hi-Lok® fastener. As a consequence, the head and collar of the fastener marginally penetrated into the outer plates and thus, led to further damage.

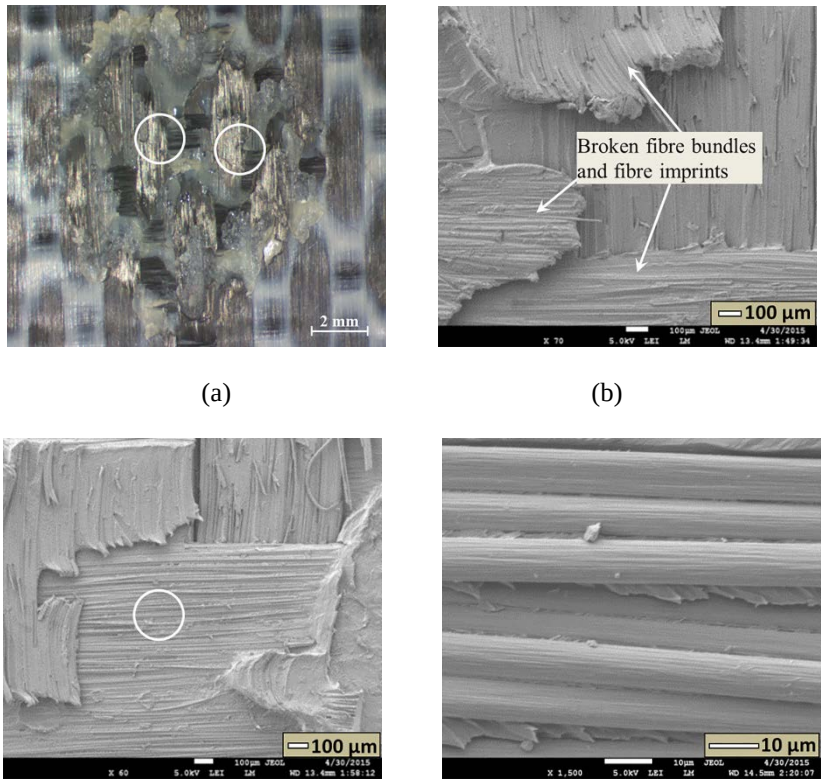

Fig. 10. Fracture surface (a) and SEM detail (b-d) for spot-welded joints after DLS tests. The left and right circles in (a) indicate the approximate locations of (b) and (c), respectively. The circle in (c) indicates the location for (d). Welding parameters: 600 J energy, 1500 N welding force, 60.8 µm peak-to-peak amplitude.

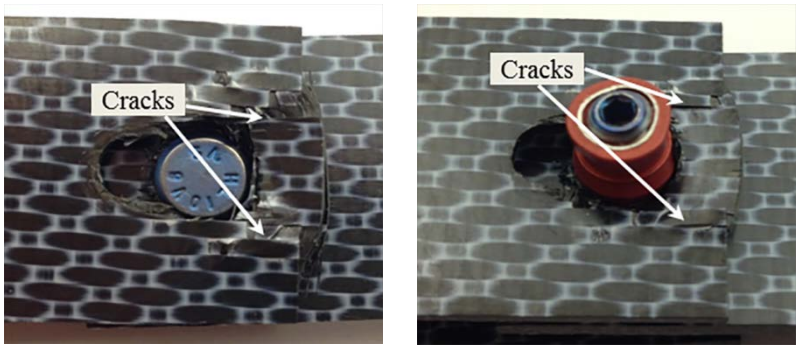

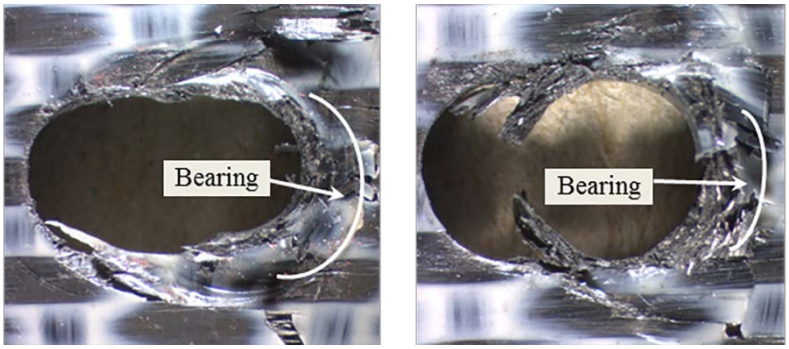

(c) (d)

Fig. 11. The top (a) and bottom (b) view of mechanically fastened joints (HL10V6) after DLS tests and fracture surfaces of outer (c) and inner (d) adherends after removing the fastener.

3.2. Mechanical behaviour of both types of joints in PT tests

Fig. 12 shows representative L-D curves for both spot-welded and mechanically fastened joints in PT tests. Similar to the DLS tests, spot-welded specimens exhibit a linear behaviour during the loading process without stiffness reduction. The averaged UFL is recorded at approximately 600 N, which is listed in Table 2, and is found to be much lower (by 82%) than the UFL of the specimens joined with HL12V6 fasteners. The OFL of mechanically fastened specimens are calculated by using the bilinear approximation method and the average value is shown in Table 2 and Fig. 13. The lower UFL of the welded joints is because the mechanically fastened joints relies on the titanium fastener (head) under peel loading, while the resistance to pull-through force of welded joints comes from the interlaminar strength of the composite adherends. As it is known that composite laminates have low transverse properties [22, 23], the observation that load-carrying capability on peel loading of welded specimens is not comparable to the mechanically fastened counterparts is as expected.

Interestingly, irrespective of the substantial difference regarding load-carrying capability, spot-welded specimens show a comparable, even slightly better, joint stiffness to the mechanically fastened specimens. Table 2 gives the experimental results of the JS of welded specimens, which is approximately 13% in excess of that of HL12V6. It is believed that welded specimens are continuous within the joints (Fig. 14(a)), which provide more constraints for the adherend bending with load increase. In contrast, more flexibility is introduced by the clearance of fastener hole, as shown in Fig. 14(b)and (c), which leads to a higher displacement and thus a lower stiffness.

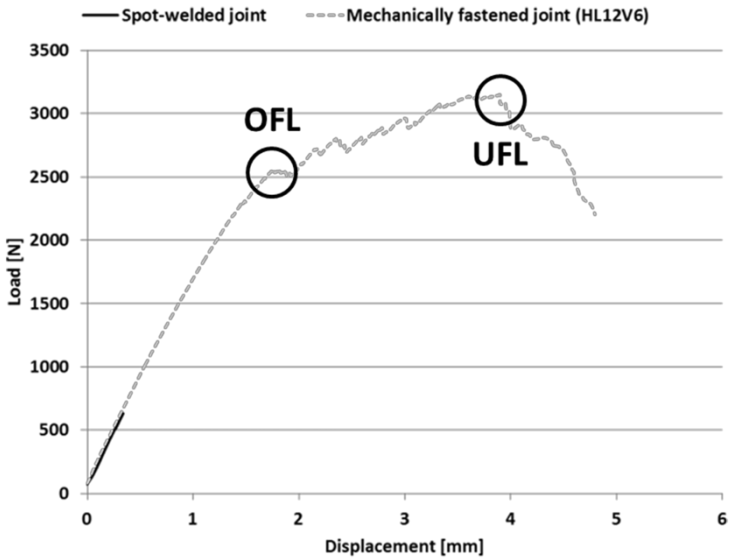

Fig. 12. Comparison of representative load-displacement curves between spot-welded (solid line) and mechanically fastened (dashed line) joints in PT tests. The left and right circles indicate the onset and ultimate failure, respectively. The data are adopted from [31].

Table 2
Experimental results on both types of joints for PT tests.

Joint type	Average OFL (N) (COV %)	Average UFL (N) (COV %)	Average JS (N/mm) (COV %)
Spot-welded joints	-	593.8 (5.1)	1622.6 (4.5)
Mechanically fastened joints (HL12V6)	2455.5 (2.3)	3190.7 (2.4)	1429.3 (6.1)

(OFL: onset failure load, UFL: ultimate failure load, JS: joint stiffness, COV: coefficient of variation)

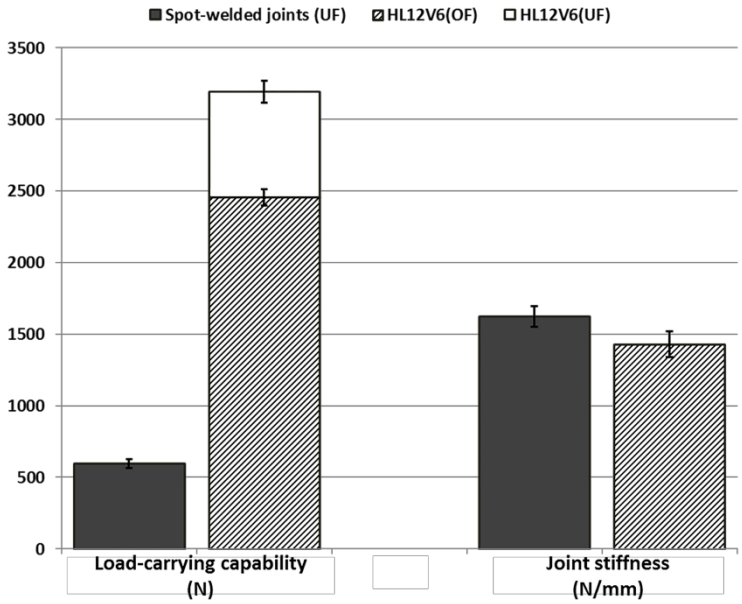

Fig. 13. Comparison of out-of-plane mechancial (peel) performance for both types of joints in PT tests. (OF: onset failure, UF: ultimate failure) The error bars indicate the standard deviation.

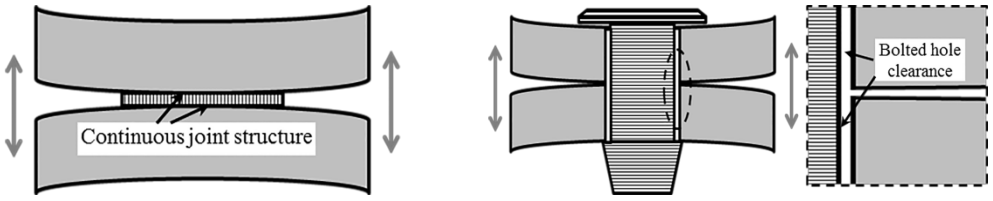

(a) (b) (c)

Fig. 14. Different boundary conditions of spot-welded (a) and mechanically fastened(b) joints in PT tests. The part of (c) is the magnification of the part in elliptical frame in (b).

Fig. 15 illustrates the fracture analysis performed on the bottom adherend of spot-welded specimens after PT tests. Similar to the observations of the DLS specimens, a circular welded joint with an approximate diameter of 10 mm was found on the fracture surface in Fig. 15(a). Fig. 15(b) gives SEM details for tearing of the out-most laminate ply. Broken fibres and fibre imprints are observed being distributed with 45° on the fracture surface, indicating they are from the out-most ply of the top adherend. Apart from that, Fig. 15(c) indicates the fibre-matrix debonding, which is shown as broken fibre bundles without little attached resin (Fig. 15(d)) resulted from the peel load. The mechanically fastened specimen in Fig. 16(a) shows the bottom plate is inserted by the Hi-Lok® collar after PT tests, which generates a local force and eventually leads to a bending failure of the laminates (Fig. 16(b)). The

bending is found in the vicinity of the bolted hole (Fig. 16(c)) whereas cracks are radially growing away from the hole (Fig. 16(d)), indicating the eventual pull-through laminate failure.

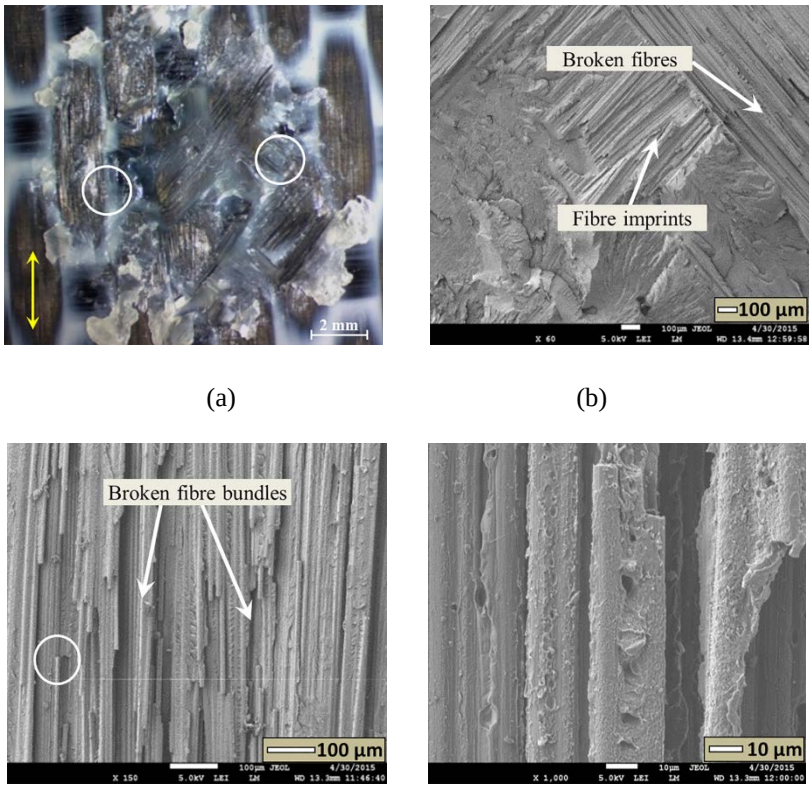

(a) (b)

(c) (d)

Fig. 15. Fracture surface (a) and SEM detail (b-d) for spot-welded joints after the PT test. The right and left circles in (a) indicate the approximate locations for (b) and (c), respectively. The circle in (c) indicates the location for (d). The apparent fibre orientation of the substrate is indicated by the vertical arrow in (a). Welding parameters: 600 J energy, 1500 N welding force, 60.8 µm peak-to-peak amplitude.

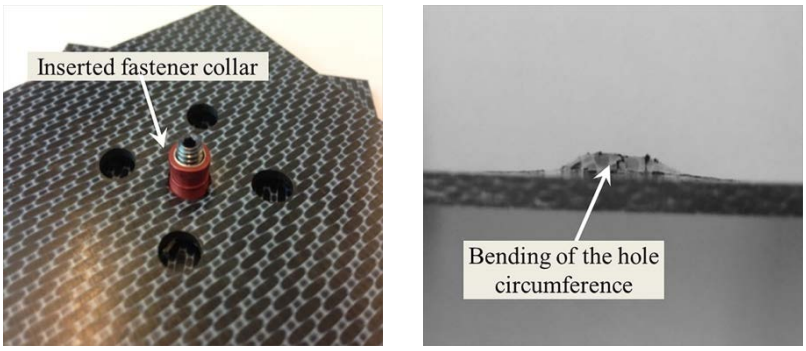

(a) (b)

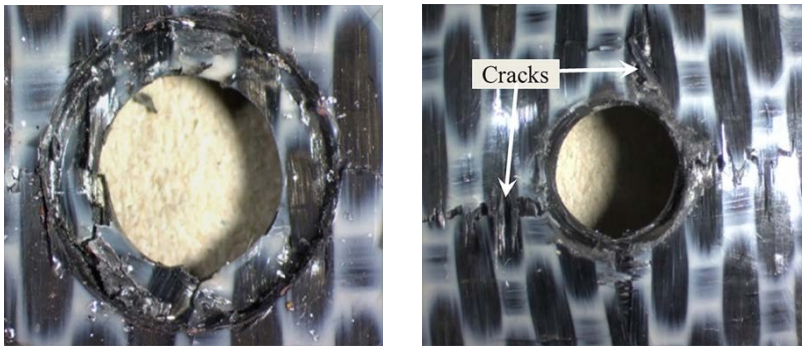

(c) (d)

Fig. 16. The Hi-Lok® collar (HL12V6) after the PT test (a) and the side (b), bottom (c) and top (d) view of fracture surface of bottom adherend after removing the fastener.

3.3. Damage affected zone

A combination of ultrasonic C-scan and cross-sectional microscopy was used to assess the internal damage in both the welded and the mechanically fastened joints. To characterize the through-the-thickness damage utilizing a microscope, some selected specimens were cross-sectioned through the central line of the overlap, parallel to the apparent fibre orientation, as indicated in Fig. 17. Afterwards, the sectioned specimens were embedded in epoxy and polished. The experimental results are separately shown based on DLS and PT tests.

3.3.1. DLS tests

The C-scan results for the overlap area of both types of joints (welded vs. mechanically fastened) after DLS tests are presented in Fig. 18. The size of the damage affected zone (DAZ) in the welded specimen is considerably smaller than the mechanically fastened counterpart. It should be noted that the damaged area captured by C-scan is restricted to the welded area (Fig. 18(a)), in correspondence with the fracture surface in Fig. 10(a). In contrast, the DAZ in mechanically fastened specimens is not only to be found in the vicinity of the fastener hole, but covers almost half of the overlap (Fig. 18(b)). The area in between the two cracks features a large amount of damage (delamination) in the laminates.

The cross-section micrographs of welded and mechanically fastened specimens provide a better characterization of the through-the-thickness damage, as shown in Fig. 19 and Fig. 20, respectively. For the welded specimen, naked fibre bundles as well as resin rich pockets are visible on the upper-most ply of the adherend in accordance with the fibre-matrix debonding failure described

before. However, this intralaminar damage is exactly limited to the first ply and no damage can be found in the rest of the adherend. Contrastingly, the laminate structure of the mechanically fastened joint is catastrophically damaged in the form of delamination and matrix cracking. The penetration of the head of the Hi-Lok® fastener results in an obvious deformation on the top. The severe interior damage of the adherend indicates that a relatively big area of material would need to be removed in order to repair the mechanically fastened joints after failure.

(a) (b)

Fig. 17. Central-cut of both welded (a) and mechanically fastened (b) specimens along the dashed lines for the cross-sectional microscopy.

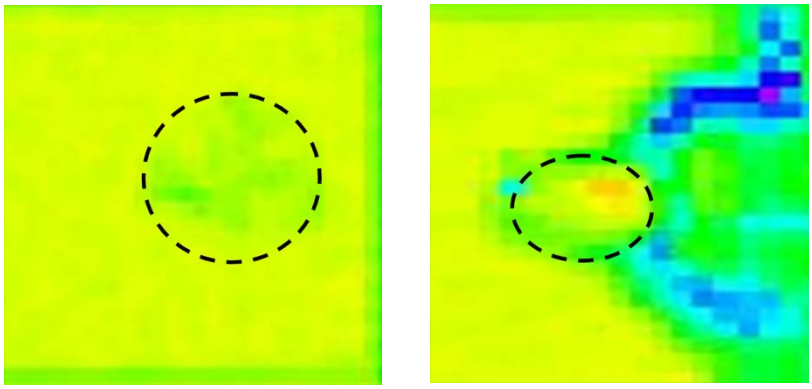

(a) (b)

Fig. 18. Comparison of damaged area of spot-welded (a) and mechanically fastened (b) joints after DLS tests. The black dashed lines indicate the welded area (a) and deformed fastener hole (b) after DLS tests, respectively.

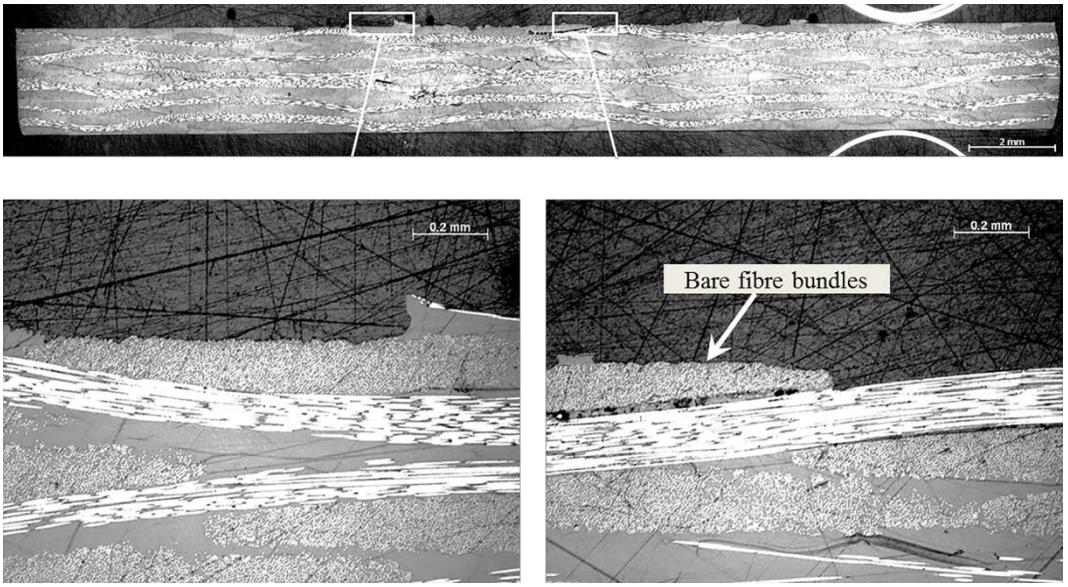

Fig. 19. Micrographic cross-sections of spot-welded joint after DLS tests. The scale bar for 2 mm is shown in the top figure. The bottom image is the magnification of the parts in the white boxes of the top one.

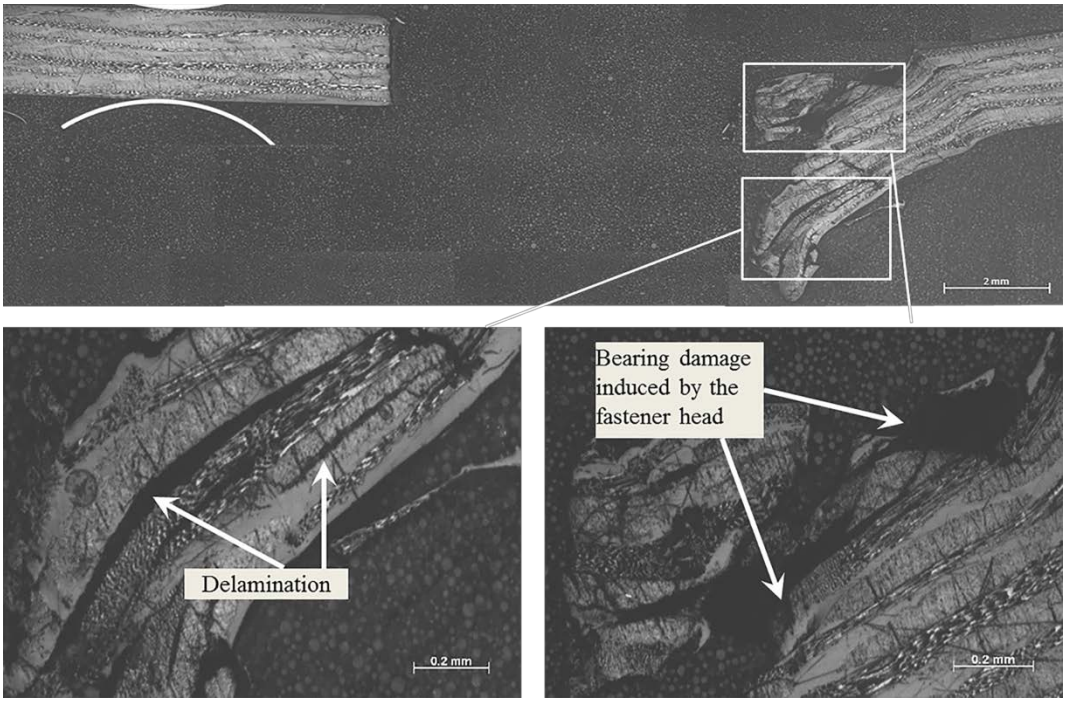

Fig. 20. Micrographic cross-sections of mechanically fastened joint (HL10V6) after DLS tests. The scale bar for 2 mm is shown in the top image. The bottom images are the magnification of the parts in the white boxes of the top one.

3.3.2. PT tests

The comparative analysis of the C-scan images for the two types of joints after the PT tests has similar results to those of the DLS specimens. The images in Fig. 21 display a

significantly larger DAZ in the mechanically fastened specimen than in the spot-welded counterpart. The DAZ of the latter is invariably limited to the welded region. Nevertheless, the internal damage in the mechanically fastened adherends is not only at the periphery of the hole but has a perceptible influence on the surrounding area, which displays a good fits with the result in [23].

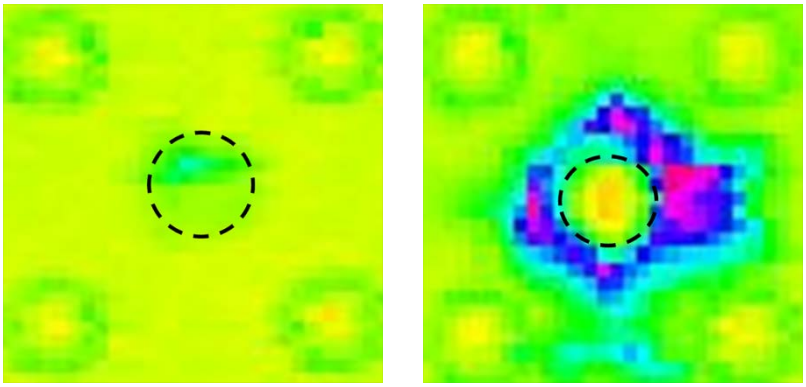

(a) (b)

Fig. 21. Comparison of damaged area of spot-welded (a) and mechanically fastened (b) joints after PT tests. The black dashed lines indicate the welded area (a) and bolted hole (b) after PT tests. The four circles at the corners are the drilled holes for loading cylinders in PT tests.

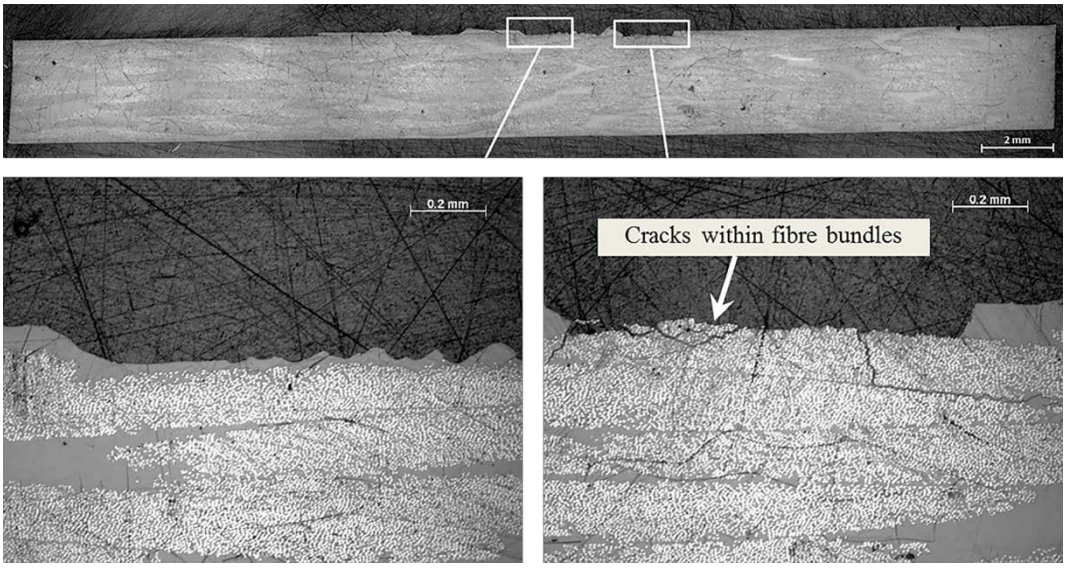

Fig. 22. Micrographic cross-sections of spot-welded joint after PT tests. The scale bar for 2 mm is shown in the top image. The bottom images are the magnification of the parts in the white boxes of the top one.

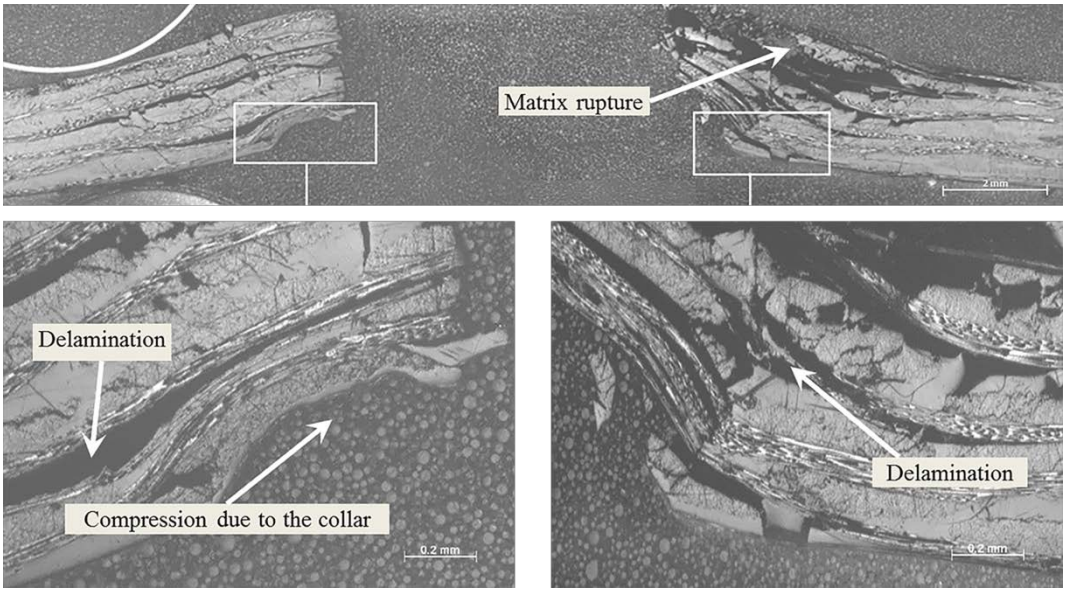

Fig. 23. Micrographic cross-sections of mechanically fastened joint (HL12V6) after PT tests. The scale bar for 2 mm is shown in the top image. The bottom images are the magnification of the part in the white boxes of the top one.

Fig. 22 shows the cross-section of the welded joint, comprised of a failure taking place both within the post-welded ED on the surface and within bare fibre bundles in the out-most ply. Conversely, matrix rupture is found on the top of the adherend of the mechanically fastened specimen due to the over-bending (Fig. 23). Furthermore, as a consequence of the insertion of the Hi-Lok® collar, the laminates are compressed in the vicinity of the fastener hole and hence delaminations are generated.

4. Conclusions

In this paper, a series of experimental studies, including two different types of mechanical tests (DLS and PT tests) and fractograpic analysis, were carried out on CF/PEEK specimens. The mechanical behaviour, failure modes and DAZ were characterized and compared between spot-welded joints and mechanically fastened joints employing Hi-Lok® fasteners. The spot welds created in both tests were found to be approximately 10 mm in diameter, which was approximately two times bigger than the original EDs as well as the employed Hi-Lok® fasteners. Additionally, based on different tests, the following conclusions can be drawn:

1. DLS tests:

- The spot-welded joints achieved a comparable load-carrying capability on shear load to the mechanically fastened joints, ranging from 94% to 112% of the average OFL of the mechanically fastened counterparts (HL10V6).
- The spot-welded joints showed an 88% higher average stiffness as compared to the mechanically fastened joints under shear loading. Extra tensile tests indicated that bearing load applied on the adherend by the fastener pin, rather than the bolted hole, is the main cause for the stiffness reduction of mechanically fastened specimens.
- Intralaminar failure was found to be the major failure mode for spot-welded joints, consisting of laminate tearing and fibre-matrix debonding. Further visual inspection by C-scan and optical microscopy indicated that failure in welded specimens was exactly restricted in the welded area and the outermost ply of the adherend. Conversely, through-the-thickness bearing damage, comprising severe delamination and matrix cracking, was introduced into the composite adherends of mechanically fastened specimens. Moreover, the damaged area was reported to be far beyond the vicinity of the bolted hole.

2. PT tests:
    - The load-carrying capability of spot-welded joints was found to be inferior to that of the mechanically fastened joints, ranging from 22%-24% of the average onset failure load of HV12V6. This is reasonable since the Hi-Lok® fastener acts as a through-the-thickness reinforcement and hence the mechanically fastened joints do not entirely rely on the through-the-thickness strength of the composite laminate to carry the peel load, as opposed to the welded joints.
    - The spot welds showed a slightly higher joint stiffness on average under peel loading, approximately 113.5% comparing to the mechanically fastened counterparts. A possible explanation is the clearance between the bolted hole and the Hi-Lok® fastener providing more flexibility for the bending of adherends.
    - Intralaminar failure was still the major failure mechanism for spot-welded joints in PT tests and neither further damaged area on surfaces nor through-the-thickness damage were observed. In

contrast, delamination was found inside the adherend of mechanically fastened specimens. Moreover, in the vicinity of the hole, laminates were severely compressed because of the penetration of the Hi-Lok® head and collar during the tests.

In general, the limited damaged area and intact adherends after joint failure for spot weld provide ease of repairing and reusability of welded structural components. In particular, for structures carrying shear load, the comparable load-carrying capability and outstanding joint stiffness provide the possibility for spot-welded joints to be a substitute for the conventional mechanical fasteners. However, the load-carrying capability of mechanically fastened joints, in particular under the peel loading, should not be discredited.

Acknowledgement

T. Zhao thanks the PhD Scholarship Fund from the China Scholarship Council (CSC) for overseas study. Part of the experimental results presented in this paper were also presented at the 17th European Conference on Composite Materials (ECCM 17), Munich/Germany, 26-30th June, 2016.

Reference

[1] Offringa AR. Thermoplastic composites-rapid process applications. Compos Part A 1996;27A:329-36.
[2] Shi H, Villegas IF and Bersee HEN. Strength and failure modes in resistance welded thermoplastic composite joints: Effect of fibre-matrix adhesion and fibre orientation. Compos Part A 2013;55:1-10.
[3] Yousefpour A, Hojjati M and Immarigeon JP. Fusion bonding/welding of thermoplastic composites. J Thermoplast Compos Mater 2004;17:303-41.
[4] Ageorges C, Ye L and Hou M. Advances in fusion bonding techniques for joining thermoplastic matrix composites a review. Compos Part A 2001;32:839-57.
[5] Stokes VK. Joining methods for plastics and plastic composites: an overview. Polym Eng Sci 1989;29(19):1310-24.
[6] Villegas IF, Moser L, Yousefpour A, Mitschang P and Bersee HE. Process and performance evaluation of ultrasonic, induction and resistance welding of advanced thermoplastic composites. J Thermoplast Compos Mater 2012;26(8):1007-24.
[7] Van Ingen JW, Buitenhuis A, Van Wijngaarden M and Simmons F, Development of the gulfstream G650 induction welded thermoplastic elevators and rudder. In: Proceedings of the international SAMPE symposium and exhibition, Seattle, WA, USA, May 2010.

[8] Xiao X, Hoa SV and Street KN. Repair of thermoplastic resin composites by fusion bonding. Composites Bonding, STP12913S, Damico DJ, Wilkins TL, and Niks SLF, Ed., ASTM International, West Conshohocken, PA, 1994. p. 30-44,
[9] Villegas IF. In situ monitoring of ultrasonic welding of thermoplastic composites through power and displacement data. J Thermoplast Compos Mater 2013;28(1):66-85.
[10] Villegas IF. Strength development versus process data in ultrasonic welding of thermoplastic composites with flat energy directors and its application to the definition of optimum processing parameters. Compos Part A 2014;65:27-37.
[11] Fukumoto S, Lum I, Biro E, Boomer R and Zhou Y. Effects of Electrode Degradation on Electrode Life in Resistance Spot Welding of Aluminum Alloy 5182. WELD J 2003:307-12.
[12] Afrin N, Chen DL, Cao X and Jahazi M. Microstructure and tensile properties of friction stir welded AZ31B magnesium alloy. Mater Sci Eng A 2008;472(1-2):179-86.
[13] Patel VK, Bhole SD, Chen DL. Ultrasonic Spot Welding of Lightweight Alloys. In: Proceedings of 13th International Conference on Fracture. Bijing, China, June 16-21, 2013. p.1-10.
[14] Prangnell P, Haddadi F and Chen YC. Ultrasonic spot welding of aluminium to steel for automotive applications—microstructure and optimisation. Mater Sci Technol 2016;27(3):617-24.
[15] Patel VK, Bhole SD and Chen DL. Microstructure and mechanical properties of dissimilar welded Mg–Al joints by ultrasonic spot welding technique. Sci Technol Weld Joining 2013;17(3):202-6.
[16] Macwan A, Patel VK, Jiang XQ, Li C, Bhole SD and Chen DL. Ultrasonic spot welding of Al/Mg/Al tri-layered clad sheets. Mater Des 2014;62:344-51.
[17] Patel VK, Bhole SD, Chen DL. Influence of ultrasonic spot welding on microstructure in a magnesium alloy. Scripta Mater 2011;65(10):911-4.
[18] Mitschang P, Velthuis R, Didi M. Induction Spot Welding of Metal/CFRPC Hybrid Joints. Adv Eng Mater 2013;15(9):804-13.
[19] Balle F, Staab F and Born J. Joining of light metals to fiber reinforced polymer composites by power ultrasonics. In: Proceedings of ECCM-17 Conference. Munich, Germany, June 26-30, 2016.
[20] Qin T, Zhao L and Zhang J. Fastener effects on mechanical behaviors of double-lap composite joints. Compos Struct 2013;100:413-23.
[21] D'Antino T, Sneed LH, Carloni C and Pellegrino C. Effect of the inherent eccentricity in single-lap direct-shear tests of PBO FRCM-concrete joints. Compos Struct 2016;142:117-29.
[22] Banbury A, Kelly DW. A study of fastener pull-through failure of composite laminates. Part 1: Experimental. Compos Struct 1999;45:241-54.
[23] Ćwik T, Iannucci L and Effenberger M. Pull-through performance of carbon fibre epoxy composites. Compos Struct 2012;94(10):3037-42.
[24] ASTM (1996) D3528-96. Standard test method for strength properties of double lap shear adhesive joints by tension loading.
[25] ASTM (2001) D5961/D5961M-01. Standard test method for bearing response of polymer matrix composite laminates.
[26] ASTM (2009) D7332/D7332M-09. Standard test method for measuring the fastener pull-through resistance of a fiber-reinforced polymer matrix composite.
[27] Catalanotti G, Camanho PP, Ghys P and Marques AT. Experimental and numerical study of fastener pull-through failure in GFRP laminates. Compos Struct 2011;94(1):239-45.
[28] de Morais AB, Pereira AB, de Moura MFSF, Silva FGA and Dourado N. Bilinear approximations to the mixed-mode I–II delamination cohesive law using an inverse method. Compos Struct 2015;122:361-6.

[29] Belnoue JPH, Giannis S, Dawson M and Hallett SR. Cohesive/adhesive failure interaction in ductile adhesive joints Part II: Quasi-static and fatigue analysis of double lap-joint specimens subjected to through-thickness compressive loading. Int J Adhes Adhes 2016;68:369-78.
[30] Hi-Shear Corporation. Hi-lok®/hi-Tigue® fastening systems installation instructions. 1991.
[31] Zhao T, Palardy G, Villegas IF, Rans C and Benedictus R. Comparative analysis of in-plane and out-of-plane mechanical behaviour of spot-welded and mechanically fastened joints in thermoplastic composites. In: Proceedings of ECCM-17 Conference. Munich, Germany, June 26-30, 2016.
[32] Villegas IF, Bersee HEN. Ultrasonic welding of advanced thermoplastic composites: An investigation on energy-directing surfaces. Adv Polym Tech 2010;29(2):112-21.

Fig. 1. Loading fixture and specimen configurations for DLS tests: (a) spot-welded specimen; (b) mechanically fastened specimen.

Fig. 2. Loading fixture and specimen configurations for PT tests: (a) spot-welded specimen; (b) mechanically fastened specimen.

Fig. 3. Bilnear approximation (dashed lines) for the OFL of mechanically fastened joints in DLS (a) and PT (b) tests. OFL is indicated by the circles on the intersection of two fitting lines.

Fig. 4. Ultrasonic welder and welding jigs used in this study. 1: circular sonotrode with a diameter of 10 mm, 2: welding jig for DLS specimens, 3: welding jig for PT specimens.

Fig. 5. Spot energy director fixed on composite adherend prior to welding process.

Fig. 6. Schematic of the Hi-Lok® fasteners utilized in the mechanical tests: (a) HL10V6; (b) HL12V6.

Fig. 7. Comparison of representative Load-displacement curves between spot-welded (solid line) and mechanically fastened (dashed line) joints in DLS tests. The left and right circles indicate the onset and ultimate failure, respectively. The data are adopted from [31].

Fig. 8. Comparison of in-plane mechanical (shear) performance for both types of joints in DLS tests. (OF: onset failure, UF: ultimate failure) The error bars indicate the standard deviation.

Fig. 9. Comparison of stiffness between intact and central-cut coupon in tensile test.

Fig. 10. Fracture surface (a) and SEM detail (b-d) for spot-welded joints after DLS tests. The left and right circles in (a) indicate the approximate locations of (b) and (c), respectively. The circle in (c) indicates the location of (d). Welding parameters: 600 J energy, 1500 N welding force, 60.8 µm peak-to-peak amplitude.

Fig. 11. The top (a) and bottom (b) view of mechanically fastened joints (HL10V6) after DLS tests and fracture surfaces of outer (c) and inner (d) adherends after removing the fastener.

Fig. 12. Comparison of representative load-displacement curves between spot-welded (solid line) and mechanically fastened (dashed line) joints in PT tests. The left and right circles indicate the onset and ultimate failure, respectively. The data are adopted from [31].

Fig. 13. Comparison of out-of-plane mechancial (peel) performance for both types of joints in PT tests. (OF: onset failure, UF: ultimate failure) The error bars indicate the standard deviation.

Fig. 14. Different boundary conditions of spot-welded (a) and mechanically fastened(b) joints in PT tests. The part of (c) is the magnification of the part in elliptical frame in (b).

Fig. 15. Fracture surface (a) and SEM detail (b-d) for spot-welded joints after the PT test. The right and left circles in (a) indicate the approximate locations of (b) and (c), respectively. The circle in (c) indicates the location of (d). The apparent fibre orientation of the adherend is indicated by the vertical arrow in (a). Welding parameters: 600 J energy, 1500 N welding force, 60.8 µm peak-to-peak amplitude.

Fig. 16. The Hi-Lok® collar (HL12V6) after the PT test (a) and the side (b), bottom (c) and top (d) view of fracture surface of bottom adherend after removing the fastener.

Fig. 17. Central-cut of both welded (a) and mechanically fastened (b) specimens along the dashed lines for the cross-sectional microscopy.

Fig. 18. Comparison of damaged area of spot-welded (a) and mechanically fastened (b) joints after DLS tests. The black dashed lines indicate the welded area (a) and deformed fastener hole (b) after DLS tests, respectively.

Fig. 19. Micrographic cross-sections of spot-welded joint after DLS tests. The bottom images are the magnification of the parts in the white boxes of the top one.

Fig. 20. Micrographic cross-sections of mechanically fastened joint (HL10V6) after DLS tests. The bottom images are the magnification of the parts in the white boxes of the top one.

Fig. 21. Comparison of damaged area of spot-welded (a) and mechanically fastened (b) joints after PT tests. The black dashed lines indicate the welded area (a) and bolted hole (b) after PT tests. The four circles at the corners are the drilled holes for loading cylinders in PT tests.

Fig. 22. Micrographic cross-sections of spot-welded joint after PT tests. The bottom images are the magnification of the parts in the white boxes of the top one.

Fig. 23. Micrographic cross-sections of mechanically fastened joint (HL12V6) after PT tests. The bottom images are the magnification of the part in the white boxes of the top one.

Table 1
Experimental results on both types of joints for DLS tests.

Joint type	Average OFL (N) (COV %)	Average UFL (N) (COV %)	Average JS (N/mm) (COV %)
Spot-welded joints	-	9645.9 (10.6)	17954.4 (3.0)
Mechanically fastened joints (HL10V6)	9190.7 (9.2)	10403.6 (7.5)	9542.5 (7.3)

(OFL: onset failure load, UFL: ultimate failure load, JS: joint stiffness, COV: coefficient of variation)

Table 2
Experimental results on both types of joints for PT tests.

Joint type	Average OFL (N) (COV %)	Average UFL (N) (COV %)	Average JS (N/mm) (COV %)
Spot-welded joints	-	593.8 (5.1)	1622.6 (4.5)
Mechanically fastened joints (HL12V6)	2455.5 (2.3)	3190.7 (2.4)	1429.3 (6.1)

(OFL: onset failure load, UFL: ultimate failure load, JS: joint stiffness, COV: coefficient of variation)